Numerical optimization of (FTO/ZnO/CdS/CH3NH3SnI3/GaAs/Au) perovskite solar cell using solar capacitance simulator with efficiency above 23% predicted

Qasim, Irfan; Ahmad, Owais; Rashid, Asim; Zehra, Tashfeen; Malik, Muhammad Imran; Rashid, Muhammad; Ahmed, M. Waqar; Nasir, M. Farooq

Published in:
Optical and Quantum Electronics

DOI:
10.1007/s11082-021-03361-5

Publication date:
2021

Optical and Quantum Electronics (2021) 53:713
https://doi.org/10.1007/s11082-021-03361-5

Numerical optimization of (FTO/ZnO/CdS/$CH_3NH_3SnI_3$/GaAs/Au) perovskite solar cell using solar capacitance simulator with efficiency above 23% predicted

Irfan Qasim[1] · Owais Ahmad[1] · Asim Rashid[2] · Tashfeen Zehra[3] · Muhammad Imran Malik[4] · Muhammad Rashid[5] · M. Waqar Ahmed[1] · M. Farooq Nasir[1]

Received: 19 July 2021 / Accepted: 2 November 2021 / Published online: 16 November 2021

Abstract

The presented study deals with the investigations of the methyl ammonium tin halide ($CH_3NH_3SnI_3$) based perovskite solar cells for optimized device performance using solar capacitance simulations software. Several necessary parameters such as metal work functions, thickness of structural layers, charge carrier's mobility and defect density have been explored to evaluate the device performance. Calculations reveal that for the best efficiency of device the maximum thickness of the perovskite ($CH_3NH_3SnI_3$) absorber layer must be 4.2 μm. The thickness values of 0.01 μm for ZnO electron transport layer (ETL), 0.871 μm for GaAs hole transport layer and 0.001 μm for CdS buffer layer have been found which proved to be optimum for maximum power conversion efficiency (PCE) of 23.80% for the device. The variation of open circuit voltage (V_{oc}), Short circuit current (J_{sc}), Fill Factor (FF %), quantum efficiency (QE) against thickness of all layers and interface defect densities in FTO/ZnO/CdS/$CH_3NH_3SnI_3$/GaAs/Au composition have been critically explored and their crucial role for the device performance has been reported. Heterojunctions between ZnO-ETL and CdS buffer layers have shown improved device performance and PCE. Current investigations may prove to be useful for designing and fabrication of climate friendly, non-toxic and highly efficient solar cells.

Keywords Perovskites · Solar cells · Absorber layer · Current density · Efficiency

✉ Irfan Qasim
dr.irfanqasim@gmail.com

[1] Faculty of Engineering and Applied Sciences (FEAS), Riphah International University, Islamabad 44000, Pakistan

[2] Transworld Solar Group, Avinguda de la Granvia 8-10, 4° – 2a, 08902 Barcelona, Spain

[3] Zernike Institute for Advanced Materials, University of Groningen, Nijenborgh 4, 9747 AG Groningen, The Netherlands

[4] School of Electrical Engineering and Computer Science (SEECS), NUST, Islamabad 44000, Pakistan

[5] Department of Physics, Ghazi University, Dera Ghazi khan, Pakistan

1 Introduction

In order to keep up with the pace of the development of modern society in the near future, the energy and power consumption will further be increased, which might result in disastrous situations. In recent years, inorganic and organo-halide solar cells with perovskite absorber materials have drawn attention in the photovoltaic community because of their outstanding photoelectric performance, high electrical parameters such as current density, quantum efficiency and low manufacturing cost (Liu et al. 2013, 2019; Deschler et al. 2014). The physical, mechanical and optoelectronic properties of perovskite materials are recommended for the photovoltaic (PV) applications. Researchers have analyzed some of these properties by using first-principle investigations with density functional theory (DFT) (Arar et al. 2015; Liu et al. 2020). A typical perovskite solar cell may employ organic–inorganic halide material as active absorber material and these types of materials exhibit efficiency of more than 20% but, there are two main concerns (Ahmed et al. 2015; Ke and Kanatzidis 2019). First, these kinds of materials consist of organic cation which create instability and thereby suppressing the life time of the perovskite material and second is the toxicity of lead (Pb) which is highly hazardous to our environment (Giustino and Snaith 2016; Li et al. 2019; Younis et al. 2020).

Replacing hazardous lead with non-toxic materials also revealed several excellent PV applications (Dai et al. 2019; Krishnamurthi et al. 2020a). Furthermore, some other challenges are also linked with such perovskite materials. For example, the open-circuit voltage of Sn^{2+} cation and Sb is quite low, oxidation of Ge^{2+} cation makes it unstable, Bi has poor charge transport ability, Cu has inferior PV properties. The maximum PCE of perovskite based solar cell is above 25%, which is quite greater than the efficiency recorded 3.8% in 2009 (Green et al. 2014; Nayak et al. 2019). This achievement has brought perovskite solar cells in photovoltaic market as compare to Si-based solar cells (Zou et al. 2018). However, some hole-transporting materials (HTM) like Spiro-OMETAD has restricted the perovskite absorber materials based solar cells to market because of their heavy manufacturing cost and suppression of long time stability (Hossain et al. 2015a). Scientists in the field of perovskite solar cells have obtained better results in the form of high mobility, absorption co-efficient and tunable band gap of the absorber layers, but still some main problems like stability degradation, toxic nature of lead, hysteresis, high cost and high-power conversion efficiency are major challenges. So, there is inexorable need to optimize the parameters of perovskite solar cells for better performance at low manufacturing cost. An active way for achieving the required results is to optimized performance of Perovskite solar cells, typically Organo-Halide Perovskite absorber materials like $CH_3NH_3XY_3$ (X = Pb, Sn, Ge & Y = Cl, Br, I) in which the major focus is to reduce toxicity and enhance stability. Numerous compositional and structural derivatives of perovskite family including layered *Ruddlesden-Popper* and double perovskites are needed to be explored on the basis of suitable theoretical, computational and experimental resources. Du et al. studied the electrical parameters and device structure stability of $CH_3NH_3SnI_3$ perovskite absorber layer by simulations. The electrical parameters such as V_{oc}, J_{sc}, FF and PCE was found to be 0.92 V, 31.59 mA/cm^2, 79.99% and 23.36% respectively. Furthermore, $CH_3NH_3SnI_3$ perovskite absorber material was found more efficient than $CH_3NH_3PbI_3$ due to non-toxicity and Sn^{+2} stability of Sn element in $CH_3NH_3SnI_3$ structure (Hui-Jing et al. 2016). Lakhdar et al. calculated the optimized PCE of 13.5% for $CH_3NH_3GeI_3$ based perovskite solar cell by inserting C_{60} as ETM layer through SCAPS-1D (Lakhdar and Hima 2019). Hima et al. reported the maximum and optimized PCE of 18.16% for $CH_3NH_3PbI_3$ solar cell and 9.56% for $CH_3NH_3SnI_3$ solar cell

by using SILVACO ATLAS simulation software (Hima et al. 2019). Abdelaziz et al. has reported the influence of defect density, layer thickness and doping concentration in iodide ($HC(NH_2)_2SnI_3$ and $FASnI_3$) based PSC through SCAPS simulation. The maximum PCE of 14.03% for optimized device was reported with V_{oc} of 0.92 V, J_{sc} of 22.65 mA/cm^2 and FF of 67.74% (Abdelaziz et al. 2020). Comprehensive device analysis for a variety of electron and hole transport layers along with variation in metal contact using $CH_3NH_3SnI_3$ perovskite as absorber material was performed by Jayan. He proposed thermodynamic stability of tin based solar cells. The device efficiency of 25.05% was achieved in Glass/FTO/PCBM/$MASnI_3$/CuI/Au configuration (Jayan and Sebastian 2021). Liu et al. studied the effect of absorber layer thickness, charge mobility and defect density on planar PSCs with efficiency over 20% using AMPS-1D (Liu et al. 2014). Yichuan et al. studied the carrier concentration and mobility of textured surface of gallium-doped zinc oxide (GZO) films based perovskite solar cell with maximum PCE of 21.132% (Chen et al. 2019). Lead free $MAGeI_3$ based perovskite solar cell showed better combination of device parameters with 18.03% efficiency in ITO/ZnO/$MAGeI_3$/Spiro-OmeTAD/Au configuration (Bhattarai and Das 2021). $CH_3NH_3SnI_3$ is a lead-free inorganic perovskite material suitable for light absorption layer due to its low energy gap of 1.35 eV, high absorption coefficient and high hole mobility of 10^4 cm^{-1} and 585 cm^2/V^{-1} s^{-1} respectively at room temperature. Sn^{2+} is a non-toxic cation as compared to Pb^{2+}ions, therefore, it is highly recommended in halide perovskite solar cells because of its excellent photoelectric performance and suitability (Hossain et al. 2015b; Rai et al. 2020; Krishnamurthi et al. 2020b).

In current research work, $CH_3NH_3SnI_3$ based PSCs have been studied and the influences of temperature, thickness of structural layers, defect densities, interface defects, carrier generation-recombination and energy band gaps have been reported for optimum device performance. The proposed novel configuration with ZnO-ETL/CdS-buffer layer heterojunctions have been explored, which may play a vital role in improved device performance due to their better optical properties. The fundamental objective of our current research work is to optimize all possible characteristic parameters of PSCs precisely and focus on getting high PCE device at reduced fabrication cost.

2 Device simulation

Device modeling and optimization of PSCs was performed by using SCAPS-1D software version (3.3.08) (Burgelman et al. 2000) under standard conditions of 100mW/cm^2 light intensity, room temperature of 300 K and AM 1.5 solar spectrum. It is a well-established windows based simulations software originally developed for polycrystalline structural layers of thin films having multiple interfaces. It was developed at the department of electronics at university of Ghent, Belgium. The algorithm of the model is based on three different coupled partial differential equations (PDEs), namely, Poisson's equation, continuity equation for holes and electrons, which are given below;

$$\begin{aligned}\frac{\partial^2\Psi}{\partial x^2} &= -\frac{\partial \mathrm{E}}{\partial x} = -\frac{\rho}{\varepsilon_s} \\ &= -\frac{q}{\varepsilon_s}\left[p - n + N_d^+ - N_a^- \pm N_{def}\right]\end{aligned} \tag{1}$$

where Ψ is electrostatic potential, ε_s is static relative permittivity, q is the charge, e and n are the respective electrons and holes, N_d^+ is donor density, N_a^- is acceptor density and N_{def}

is the defect density of both donor and acceptor. The carrier continuity equation in device may be represented as given below;

$$-\frac{\partial j_p}{\partial x} + G - U_p(n,p) = 0 \tag{2}$$

and

$$-\frac{\partial j_n}{\partial x} + G - U_n(n,p) = 0 \tag{3}$$

Here j_p and j_n are the hole and electron current densities, G is carrier generation rate, U_n (n, p) and U_p (n, P) are the recombination rates of electrons and holes respectively. Furthermore, carrier current density may also be obtained from;

$$j_p = qn\mu_p E - qD_p\frac{\partial p}{\partial x} \tag{4}$$

$$j_n = qn\mu_n E + qD_n\frac{\partial n}{\partial x} \tag{5}$$

Here q is the charge, $\mu_p and \mu_n$ are carrier mobilities and D_p, D_n are the diffusion coefficients. Several photovoltaic electrical parameters may be calculated such as current density (J_{sc}), open circuit voltage (V_{oc}), percentage PCE and fill factor (FF %) against various thickness values at wide range of temperatures. In SCAPS-1D seven structural layers may be accommodated in solar cell composition, which can work both in light and dark environments (Karimi et al. 2017; Hima et al. 2019). In the proposed device configuration FTO/ZnO/CdS/$CH_3NH_3SnI_3$/GaAs/Au of solar cell $CH_3NH_3SnI_3$ layer acts as light harvesting absorber material, inserted between GaAs-HTL and Buffer Layer (CdS) along with ZnO-ETL. Due to remarkable results reported in previous literature, Fluorine doped tin oxide (FTO) is used as front contact and gold (Au) thin layer as back metal contact.

3 Simulation methodology

The architecture model and device structure used for simulated solar cell FTO/ZnO/CdS/$CH_3NH_3SnI_3$/GaAs/Au is illustrated in Fig. 1. In this configuration, the work functions of Au and FTO have been taken from the literature i.e. 5.1 eV for Au and 4.4 eV for FTO material. The standard working procedure involving characteristic steps was followed to carry out optimization and evaluation process of the device. The input material parameter for structural layer were calculated by density functional theory (DFT) studies and were compared with various available literatures for simulations purpose and as shown in Table 1. And the thickness of each layer was optimized for maximum device output.

The interfacial defects for first interface CdS/$CH_3NH_3SnI_3$ and 2nd interface $CH_3NH_3SnI_3$/GaAs were also inserted and analyzed during simulations with parameters shown in Table 2. Initially the arbitrary thickness of ZnO layer was set 0.07 µm, $CH_3NH_3SnI_3$-Peroskite layer 0.4 µm and GaAs layer 1 µm. The processes of optimizations of layer thickness were obtained by changing the thickness of one layer and keep constant the thickness of other two layers. The maximum PCE was investigated for optimized layer thickness values. Similarly, the batch parameters setting for each layer thickness were also varied. At first, ZnO

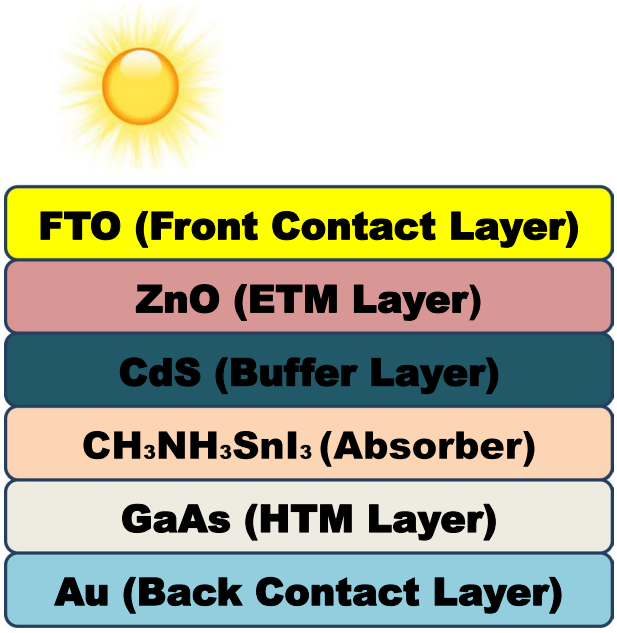

Fig. 1 Simulated diagram of $CH_3NH_3SnI_3$-based perovskite solar cell

Table 1 Material parameters of ETM layer, Buffer layer, $CH_3NH_3SnI_3$ absorber layer and HTM layer

Material parameters	ZnO (ETM)	CdS (Buffer)	$CH_3NH_3SnI_3$ (Absorber)	GaAs (HTM)
Thickness (μm)	0.01(variable)	0.001(variable)	0.2 (variable)	1.00 (variable)
Energy band-gap (eV)	3.37	2.44	1.35	1.42
Electron Affinity	4.35	4.40	4.170	4.07
Dielectric Permittivity	10.0	10.00	6.50	12.9
CB DOS	2.22×10^{18}	2.2×10^{18}	1.0×10^{18}	2.2×10^{18}
VB DOS	1.78×10^{19}	1.8×10^{19}	1.0×10^{19}	1.8×10^{19}
Electron/hole thermal velocity	1×10^{7}	1×10^{7}	1×10^{7}	1×10^{7}
Electron Mobility	100	100	10.0	8500
Hole Mobility	25	25	10.0	400
N_d	1E20	1E18	0	0
N_a	0	0	3.20×15	1.0×11

layer thickness was varied from 0.010 to 4.00 μm and maximum PCE was noted corresponding to optimized layer thickness of ZnO. Then $CH_3NH_3SnI_3$-Peroskite layer was varied from 0.200 to 5.00 μm and maximum PCE was noted corresponding to optimized layer thickness of $CH_3NH_3SnI_3$-Peroskite. Keeping constant the layer thickness of ZnO and $CH_3NH_3SnI_3$-Peroskite layer, the thickness of GaAs was varied from 0.050 to 6.000 μm and maximum PCE was noted corresponding to optimized layer thickness (Ye et al. 2016). Similarly, keeping constant the thickness values of all structural layers, the thickness of CdS layer

Table 2 Material parameters of interface defects of layers

Material parameters	CdS/ZnO	CdS/ $CH_3NH_3SnI_3$ layer	$CH_3NH_3SnI_3$/ GaAs layer
Defect type	Neutral	Neutral	Neutral
Capture cross section for Electrons and holes/(cm^2)	1.0×10^{-15}	1.0×10^{-15}	1.0×10^{-15}
Energy distribution	Single	Single	Single
E- level w.r.t E_v (above E_v, eV)	0.6	0.6	0.6
Total density N_t/cm^3	1.0×10^{19}	1.0×10^{16}	1.0×10^{13}

was varied from 0.001 to 1 µm. Finally, we found the optimized results for FTO/ZnO/CdS/ $CH_3NH_3SnI_3$/GaAs/Au solar cell device against optimized layers thickness values.

4 Results and discussion

4.1 Optimized electrical parameters of $CH_3NH_3SnI_3$-based perovskite solar cell

The electrical parameters and characteristic thickness values of all structural layers were delicately examined to achieve optimum device parameters. The energy band alignment diagram of optimized device is shown in Fig. 2. Beyond these values, even a slight variation in the inserted layers parameters may suppress the performance of device. The J–V characteristics of the solar cell are presented in Fig. 3. It is observed that at optimized thickness values of ETL/ Buffer/Absorber/HTL layers of solar cell, the observed open circuit voltage (V_{oc}) has been observed to be 0.9602 V, short circuit current density (J_{sc}) value was found to be 33.8608 mA/ cm^2 and an improved 73.20% value of fill factor. These performance results have been attained at optimum parameters of the device.

The overall layout of the maximum device performance for various parameters is represented in Fig. 4. The energy band gaps were fine tuned to achieve the values of 1.42 eV for GaAs, 1.35 eV for $CH_3NH_3SnI_3$- absorber, 2.44 eV for CdS layer and 3.370 eV for ZnO-ETL. Fluorine doped Tin Oxide with work function (φ = 4.4 eV) and Gold (Au) metal contacts (φ = 5.1 eV) were used for optimized device output.

The carrier mobility of the absorber layer has a remarkable effect on the device performance. Low hole mobility causes a high series resistance and thus restrict the current in the device, leading to an undesirable performance. The PCE% for $CH_3NH_3SnI_3$ perovskite absorber is observed to be increasing for enhanced values of hole and electron mobilities. A more detailed interpretation related to the trade-off between carrier recombination rate and carrier mobility and can be understood as follow. Considering the equation;

$$V_{oc} = ln\left(\frac{J_{sc}}{J_o} + 1\right)\frac{KT}{q} \tag{6}$$

According to the Einstein equation

$$\frac{\mu}{KT} = D_{n,p} \tag{7}$$

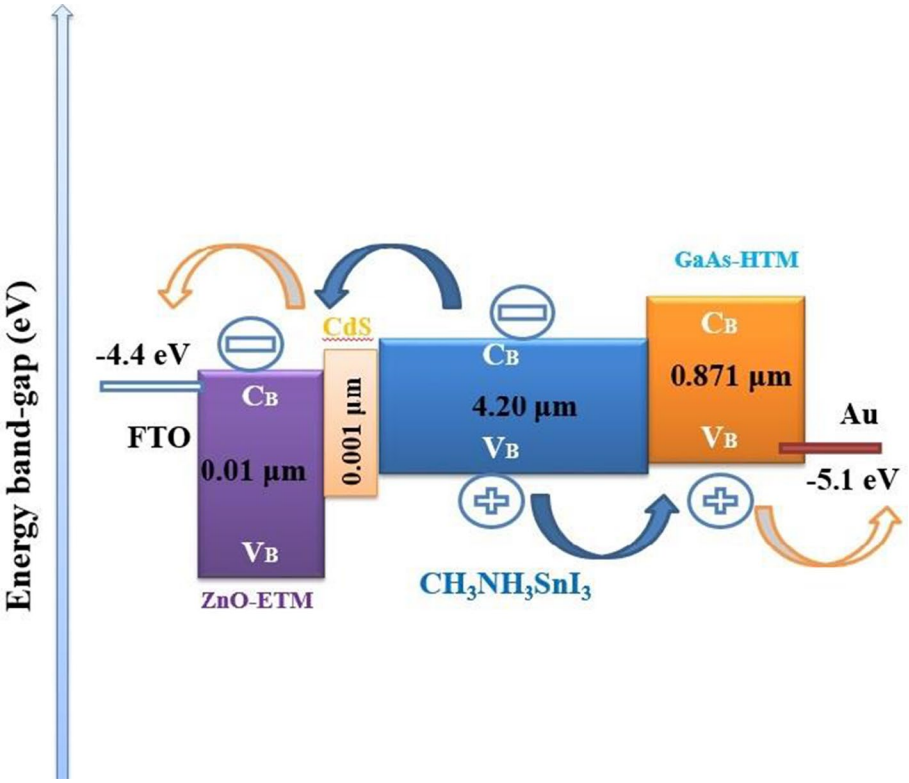

Fig. 2 Band alignment and thickness information of optimized architecture

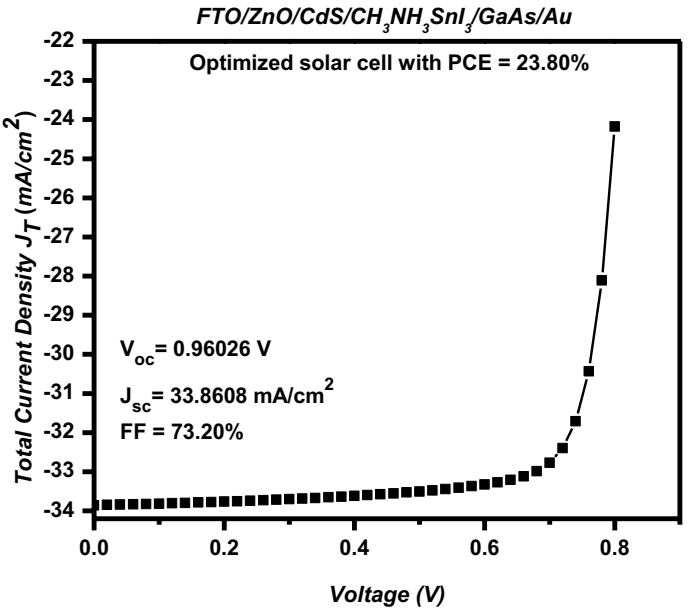

Fig. 3 J-V characteristics for the optimized perovskite Solar cell

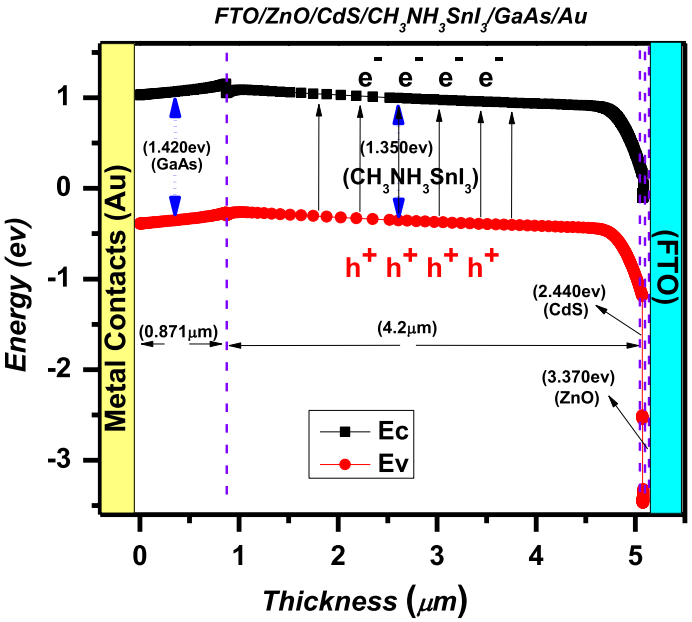

Fig. 4 Optimized device energy band diagram

A larger mobility (μ) means a larger diffusion coefficient (D), a larger reverse saturation current J_{sc}, when temperature (T), diffusion length and doping concentration stay constant. It may be observed that, a larger mobility may lead to an increased current density and decreased V_{oc}, which directly suppressed PCE. This suggests that, for high performance solar cells, a low electron carrier recombination rate is relatively more important than a high electron carrier mobility (Huang et al. 2016; Anwar et al. 2017). The interface defect layers for GaAs/$CH_3NH_3SnI_3$, ZnO/CdS and $CH_3NH_3SnI_3$/CdS interfaces have been considered for the simulations of the proposed perovskite solar cells. Numerical simulation has been performed on the defect density at interfaces in range of 1.0×10^{10} to 1.0×10^{19} cm^{-3}. Figure 5 shows histogram bars for all interfaces defect densities versus PCE for optimized perovskite solar cell. From the figure, it can be deduced that increasing interface defect densities, the recombination rate also improves which in turn reduces the PCE. The higher defect densities of the interfaces bring more traps and recombination centers, and deteriorate the performance of cells. So, it can be realized from the simulated results that interface defect density of 1×10^{10} cm^{-3} is optimum for device simulation. Figure 6 shows the relationship of carrier's recombination (cm^{-3} s) and diffusion length (μm) of the optimized solar cell. G_{eh} of 13.64×10^{21} cm^{-3} s is found to be maximum at 5.07 μm. Also, it is clear that with the enhancement of diffusion length, carrier's recombination also increases and thus will degrade the performance of solar cell (Zekry et al. 2018). Furthermore, SRH recombination and total recombination are approximately equal and are found to be maximum at 4.226×10^{17} cm^{-3} s. The quantum efficiency versus the wavelength of incident radiations is represented in Fig. 7. The illumination intensity of solar radiations in solar spectrum is found maximum for the selected wavelength range, therefore, it is illustrated that maximum absorption is in visible region of wavelength along with

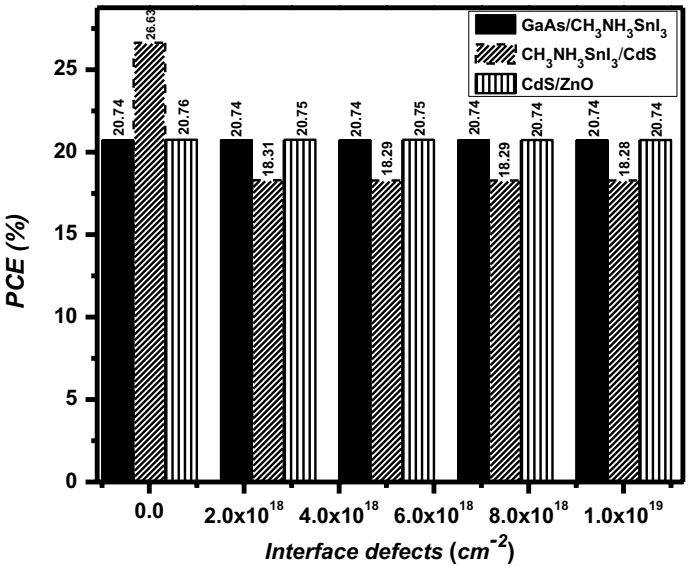

Fig. 5 Interface defect density Vs PCE (%) diagram

some part of absorption in ultraviolet and infrared regions. The high value of quantum efficiency means better absorption of the light. Degradation in efficiency is noticed in far-infrared region of wavelength. Lower the wavelength of incident radiations, greater is their absorption. Beyond these limits a suppression in device performance is observed. Quantum efficiency of 23.80%, current density (J_{sc}) of 33.8608 mA/cm^2, open circuit voltage (V_{oc}) of 0.9602 V and Fill Factor (FF) of 73.20% is observed for the optimized FTO/ZnO/CdS/$CH_3NH_3SnI_3$/GaAs/Au solar cell.

4.2 Effects of ZnO electron transport layer thickness

The effect of thickness of the electron transport layer (ZnO) on device performance has been studied using SCAPS-1D. It has been observed that as the thickness of ZnO Layer increases from 0.010 to 2.000 µm in thirty steps, the open circuit voltage (V_{oc}), short-circuit current density (J_{sc}), Fill Factor (FF) and quantum efficiency (eta%) was slightly reduced and then became constant from 2.00 to 4.00 µm. The variation of electrical parameters (V_{oc}, J_{sc}, FF% and PCE%) versus thickness for ZnO layer correspond to layer thickness is illustrated in Fig. 8. The maximum values of electrical parameters such as efficiency, short-circuit current density, open circuit voltage and Fill Factor were recorded 15.46%, 29.45269 mA/cm^2, 0.75692 V and 69.36% respectively at 0.010 µm. It means that the electrical parameters of the organic–inorganic perovskite-based solar cell are not too much affected by electron transport layer (ETL) (Kang et al. 2019). This is explained on the basis of the fact that perovskite compound itself may help the generation of charge carriers by photon excitation and ETL layer is just a charge transport layer.

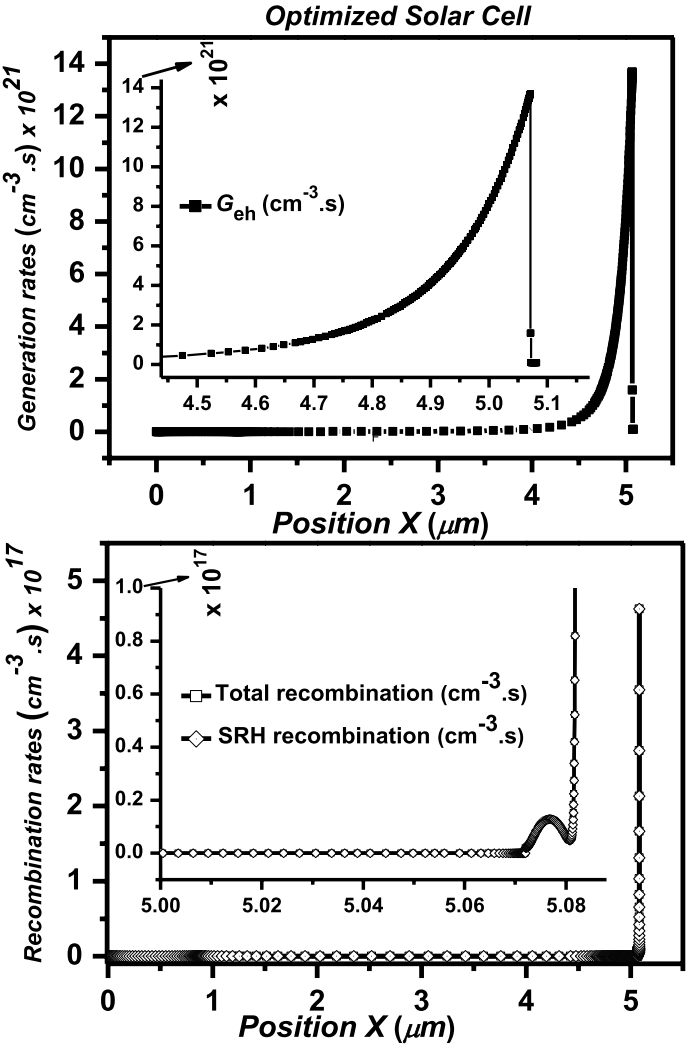

Fig. 6 Carrier generation & recombination rates versus thickness of optimized solar cell

4.3 Effects of CdS buffer layer thickness

From the technological point of view, to make the solar cells more efficient there is requirement of space charge region of high crystallinity, where the carriers in the form of electron and holes get separated. The size of this region must be comparable to the inverse coefficient of absorption and the thickness of this region should be small, so that carrier recombination may not occur. The buffer layer determines the width of the space charge region. In the proposed solar cell configuration FTO/ZnO/CdS/$CH_3NH_3SnI_3$/GaAs/Au, the requirement of space charge region has been fulfilled by CdS buffer layer. The variation in thickness of this layer considerably influence the electrical parameters of the solar cell as shown in the Fig. 9. The increase of CdS layer thickness reduced all the electrical parameters (J_{sc}, V_{oc}, PCE %) except FF%. The possible reason for the improvement in FF may

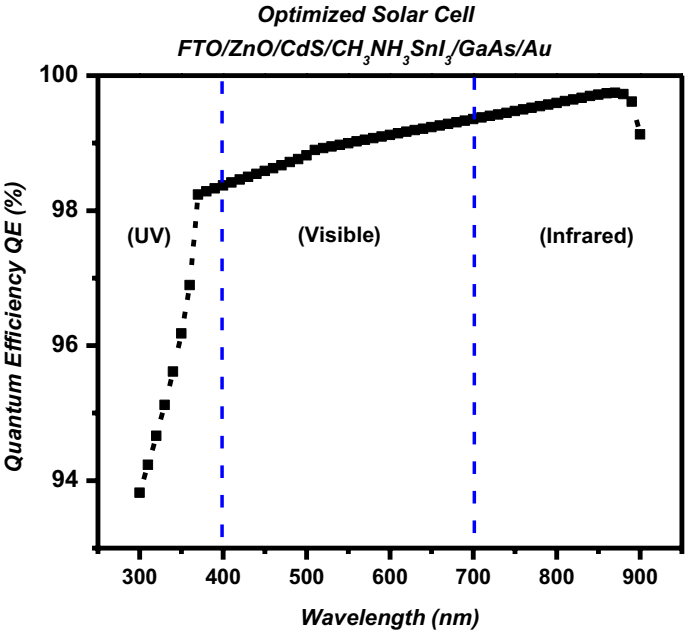

Fig. 7 Quantum efficiency (QE %) vs wavelength

be the role of CdS layer in reducing the carrier recombination which ultimately increase the area under the voltage versus current density curve. The highest values for J_{sc}, V_{oc}, FF%, PCE% were recorded ~ 31.626980 mA/cm^2, 0.9215 V, 61.11% and 17.81% at 1 nm thickness.

4.4 Effects of $CH_3NH_3SnI_3$ absorber layer thickness

The thickness of the $CH_3NH_3SnI_3$ (light-absorber layer) versus different electrical parameters is shown in Fig. 10. The power conversion efficiency (PCE), current density (J_{sc}) and open circuit voltage (V_{oc}) gradually increases with the increase of layer thickness. The maximum PCE, current density J_{sc} and open circuit voltage V_{oc} were recorded 20.73%, 33.766332 mA/cm^2 and 0.7683 V corresponds to optimized light-absorber layer thickness of 4.20 µm. The maximum value of achieved FF is fund to be 80.276%. This happens because the enhanced efficiency is due to the increase in the current density as the light-absorber layer thickness is increased. The increase in absorber layer thickness helps in enhancing the carrier generation due to more exposure of the absorber material to light (Minemoto 2014; Hui-Jing et al. 2016; Das and Paul 2020). More electron–hole pairs are generated and thereby electron mobility is increased as shown by the increased J_{sc}. The only electrical parameter Fill Factor (FF%) initially increases up to 80.276% at 3.40 µm but then gradually decreases as the layer thickness is increased up to 5.0 µm. This can be due to the recombination of the charge carriers and reduction in lifetime of the charge carrier in the $CH_3NH_3SnI_3$-perovskite layer. The recorded electrical parameters for various layer thicknesses were rechecked and confirmed.

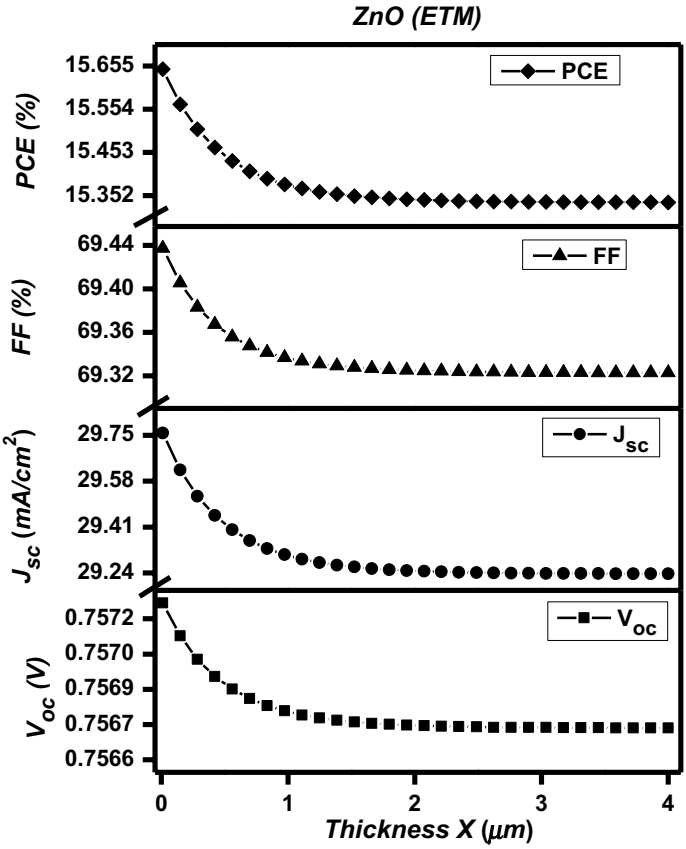

Fig. 8 (V_{oc}, J_{sc}, FF and PCE) vs thickness for ZnO electron transport layer

4.5 Effects of GaAs hole transport layer thickness

Properties like high efficiency, flexibility and light weight, resistance to UV radiation and moisture and a low temperature coefficient make gallium arsenide (GaAs) more favorable than the ubiquitously-used silicon for solar cells. In this study, GaAs is acting as a hole transport layer in device structure as shown in Fig. 11. The variation of thickness of GaAs layer from 0.050 to 6.00 μm has been studied on perovskite solar cell. The maximum power conversion efficiency (PCE) was found to be 15.6071% against the optimized thickness of 0.871 μm. The Fill Factor (FF%) gradually increases with the increase of thickness and was found to be maximum up to 69.43%. While the current density (J_{sc}), open circuit voltage (V_{oc}) and power conversion efficiency (PCE) initially enhances with the enhancement of thickness but then suppressed as the thickness is further increased up to 6 μm. The behavior of V_{oc}, J_{sc}, FF% and PCE% can be seen in Fig. 11. All the electrical parameters such as J_{sc}, PCE, V_{oc} and FF% correspond to layer thickness of GaAs layer were re-verified.

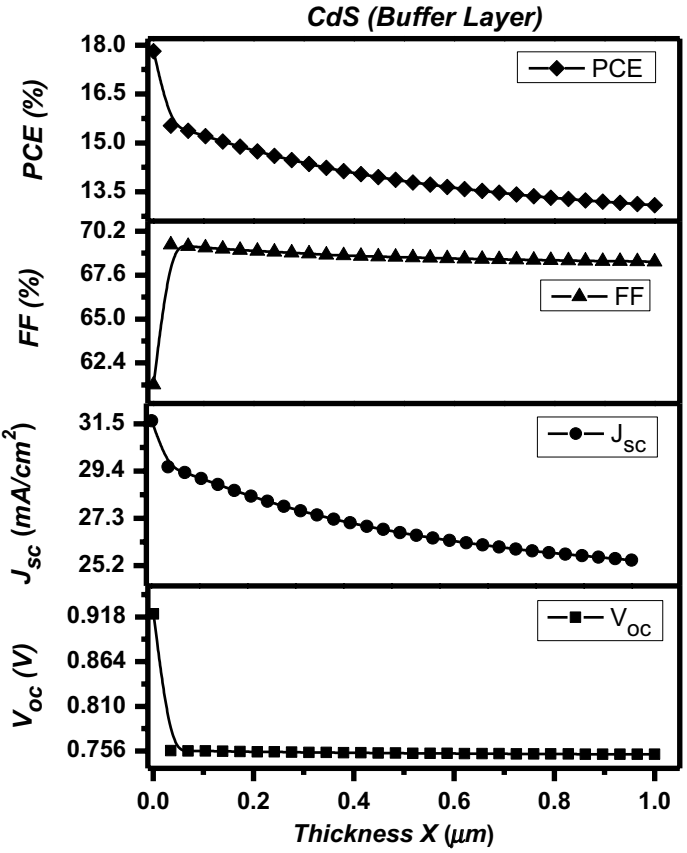

Fig. 9 (V_{oc}, J_{sc}, FF and PCE) vs thickness for CdS buffer transport layer

4.6 Effects of temperature on optimized $CH_3NH_3SnI_3$-based solar cell

Solar cells are greatly affected by temperature T(K) when exposed to sunlight. It is important to investigate the performance of optimized solar cells as a function of temperature T(K). The temperature dependence of electrical parameters for optimized perovskite solar cells are shown in Fig. 12. There is initially increasing trend in the FF% and after 300 K there is continuous decrease in its value. Practically, the rise in temperature give rise to carrier creation but, at the same time higher phonon movements and collisions also play dominant role in reduction of FF PCE and V_{oc}. For the rise in FF% the possible reason may be higher stability, higher thickness value and reduced recombination rate and lifetimes associated with carriers in $CH_3NH_3SnI_3$ absorber. A critical review of the results indicates that there is enhancement in the value of current density from 33.11 to 35.9817 mA/cm^2 with rise in temperature up to 340 K. The increase in J_{sc} may be due to the fact that higher temperatures lead to lattice expansion and attenuation of interatomic bonds. Consequently, higher cell temperatures result in a shrinking of the energy band gap, which means more photons are absorbed, which in turn, leads to free charge carriers being produced. That inferred a greater flow of electrons (i.e., more current is generated) with low energies (i.e.,

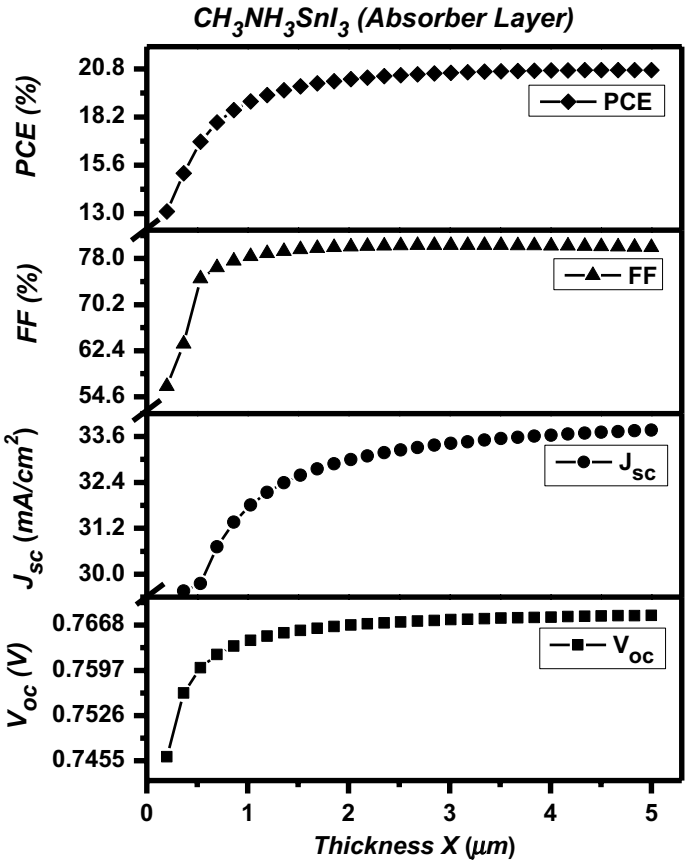

Fig. 10 (V_{oc}, J_{sc}, FF and PCE) vs thickness of $CH_3NH_3SnI_3$ absorber layer

a drop-in voltage). Therefore, this leads to decreases in voltage. On the other hand, however, the rise in current leads to a reduction in maximum power, fill factor, as well as the conversion efficiency. The suggested thickness value 4.2 μm of $CH_3NH_3SnI_3$ absorber, help in maintain longer carrier life time and CdS window layer help reducing carrier recombination to some extent which ultimately help in covering more area under J_{sc} Versus V_{oc} curve indicating improved FF%. Slight reduction in V_{oc} may also be attributed to presence of CdS buffer layer which cause parasitic absorption with increasing thickness. The lower wavelength photons are perturbed to reach the absorber layer which ultimately reduce output current, V_{oc} and overall efficiency.

5 Conclusion

In our current study, FTO/ZnO/CdS/$CH_3NH_3SnI_3$/GaAs/Au perovskite solar cell was systematically optimized and studied for better power conversion efficiency (PCE) and current density (J_{sc}) using SCAPS-1D simulation software. The influence of change in layer thickness of $CH_3NH_3SnI_3$ (Absorber Layer), ZnO (ETM Layer), GaAs (HTM Layer) and CdS (Buffer

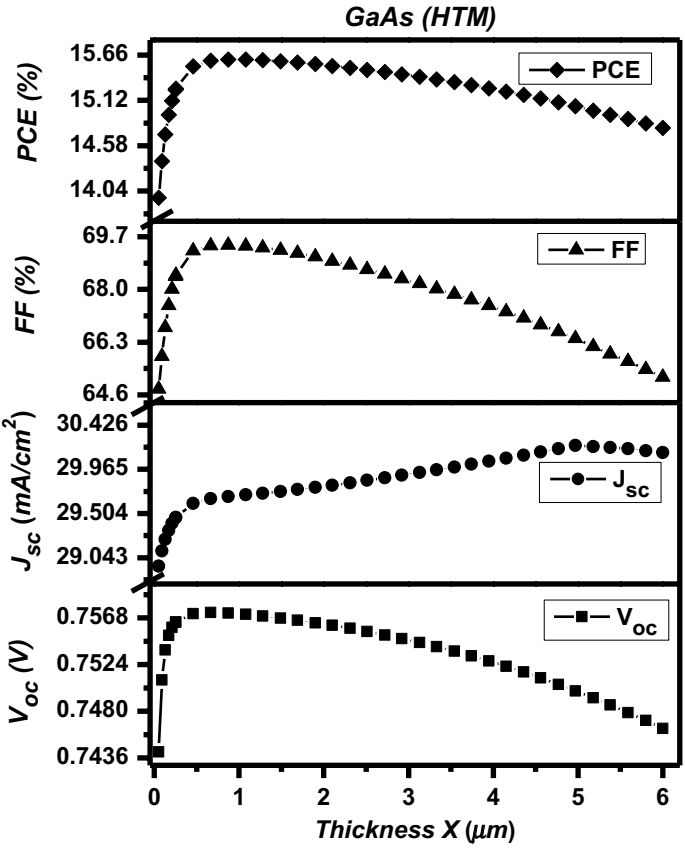

Fig. 11 (V_{oc}, J_{sc}, FF and PCE) vs thickness for GaAs hole transport layer

Layer) on the electrical parameters were optimized at values 4.200 μm, 0.01 μm, 0.871 μm and 0.001 μm respectively with a better power conversion efficiency (PCE), current density, open circuit voltage and Fill Factor of ~ 23.80%, 33.8608 mA/cm^2, 0.9602 V and 73.20% respectively. The PCE of GaAs-HTL and $CH_3NH_3SnI_3$-absorber increases with the increase of hole and electron mobilities, whereas the PCE of CdS-Buffer and ZnO-ETL suppress with the increase of hole mobility. The effects of interface defect density versus PCE show no effect on efficiency for $CH_3NH_3SnI_3$/GaAs and ZnO/CdS interfaces. The effect of energy band-gap tuning of individual layer for optimized performance showed improved PCE for energy band-gap values of 1.42 eV for GaAs, 1.35 eV for $CH_3NH_3SnI_3$-absorber, 2.44 eV for CdS-Buffer and 3.37 eV for ZnO-ETL. This may happen due to the stronger recombination of charge carriers at interfaces before being collected. The enhancement of diffusion length increased the carrier's recombination rate and thus degraded the performance of solar cell. Furthermore, maximum efficient performance of the device is observed in temperature range of 270 K–280 K. These results emphasize the need to improve and enhance the research being carried out in sustainable energy sector and particularly in multi-layer organic and inorganic halide solar cells. GaAs hole transport layer in photovoltaics, can potentially lead to light-weight, inexpensive and scalable solar cell manufacturing, ZnO as electron extraction layer along with CdS buffer layer in photovoltaic devices may carry high mobility and low processing cost. Also,

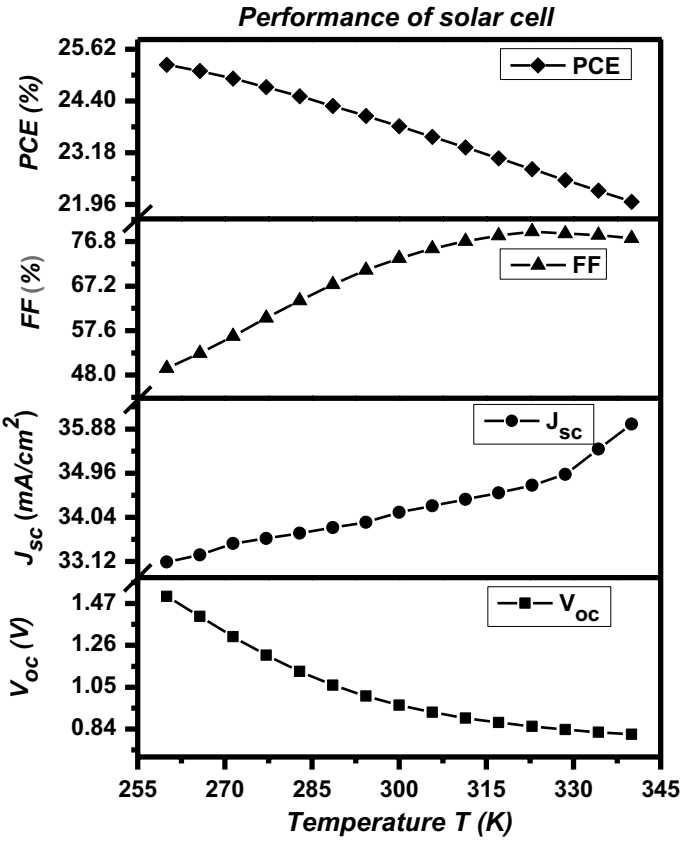

Fig. 12 (V_{oc}, J_{sc}, FF and PCE) vs temperature for optimized solar cell

$CH_3NH_3SnI_3$ perovskite absorber is environment friendly and stable. The role of ZnO/CdS heterojunction may significantly improve the device performance. The proposed solar cell configuration FTO/ZnO/CdS/$CH_3NH_3SnI_3$/GaAs/Au may deliver better results to be used for lead-free $CH_3NH_3SnI_3$ based solar devices in terms of better power conversion efficiency and improved electrical parameters.

Acknowledgements The authors are thankful to the Marc. Burgelman and his team at the electronics and Information Systems (ELIS), University of Gent, Belgium for provision of access to SCAPS software.

Declarations

Conflict of interest The authors declare that they have no known competing financial interests or personal relationships that could have appeared to influence the work reported in this paper.

References

Abdelaziz, S., Zekry, A.A., Shaker, A., Abouelatta-Ebrahim, M.: Investigating the performance of formamidinium tin-based perovskite solar cell by SCAPS device simulation. Opt. Mater. **101**, 109738 (2020). https://doi.org/10.1016/j.optmat.2020.109738

Ahmed, M.I., Habib, A., Javaid, S.S.: Perovskite solar cells: potentials, challenges and opportunities. Int. J. Photo Energy (2015). https://doi.org/10.1155/2015/592308

Anwar, F., Mahbub, R., Satter, S.S., Ullah, S.M.: Int. J. Photoenergy **2017**, 9 Article ID 9846310. https://doi.org/10.1155/2017/9846310

Arar, R., Ouahrani, T., Varshney, D., Khenata, R., Murtaza, G., Rached, D., Bouhemadou, A., Al-Douri, Y., Bin Oman, S., Reshak, A.H.: Structural, mechanical and electronic properties of sodium based fluroperovskites NaXF3 (X= Mg, Zn) from first-principle calculations. Mater. Sci. Semi. Pro. **33**, 127–135 (2015). https://doi.org/10.1016/j.mssp.2015.01.040

Bhattarai, S., Das, T.D.: Optimization of carrier transport materials for the performance enhancement of MAGeI3 based perovskite solar cell. Solar Energy **217**, 200–20 (2021). https://doi.org/10.1016/j.solener.2021.02.002

Burgelman, M., Nollet, P., Degrave, S.: Modelling polycrystalline semiconductor solar cells. Thin Solid Films. **361–362**, 527–532 (2000). https://doi.org/10.1016/S0040-6090(99)00825-1

Chen, Y., Yuehui, Hu., Meng, Qi., Yan, H., Shuai, W., Zhang, Z.: Continuous size of tuning of mono dispersed Zno nanoparticlesand its size effects on the performance of perovskite solar cells. J. Mater. Sci.: Mater. Electron. **30**, 4726–4736 (2019). https://doi.org/10.1021/acsami.7b00726

Dai, Z., Ou, Q., Wang, C., Si, G., Shabbir, B., Zheng, C., Wang, Z., Zhang, Y., Huang, Y., Bao, Q.: Capillary-bridge mediated assembly of aligned perovskite quantum dots for high-performance photodetectors. J. Mater. Chem. C **7**(20), 5954–5961 (2019). https://doi.org/10.1039/C9TC01104H

Das, N., Paul R.: Int. Res. J. Moderniz. Eng. Technol. Sci. **02**(08/A) (2020)

Deepthi Jayan, K., Sebastian, V.: Comprehensive device modelling and performance analysis of $MASnI_3$ based perovskite solar cells with diverse, ETM, HTM, and back metal contacts. Solar Energy **217**, 40–48 (2021). https://doi.org/10.1088/1361-6641/abf46c

Deschler, F., Price, M., Pathak, S.: High photo luminescence efficiency and optically pumped lasing in solution-processed mixed halide perovskite semi-conductors. J. Phys. Chem. Lett. **5**(8), 1421–1426 (2014). https://doi.org/10.1021/jz5005285

Giustino, F., Snaith, H.J.: Toward lead-free perovskite soar cells. ACS Energy Lett. **1**, 1233–1240 (2016). https://doi.org/10.1021/acsenergylett.6b00499

Green, M.A., Ho-Baillie, A., Snaith, H.J.: The emergence of perovskite solar cells. Nat. Photon. **8**, 506–514 (2014). https://doi.org/10.1038/NPHOTON.2014.134

Hima, A., Lakhdar, N., Benhaoua, B., Saadoune, A., Kemerchou, I., Rogti, F.: An optimized perovskite solar cell designs for high conversion efficiency. Superlattices Microstruct. **129**(2019), 240–246 (2019). https://doi.org/10.1016/j.spmi.2019.04.007

Hima, A., Lakhdar, N., Benhaoua, B., Saadoune, A., Kemerchou, I., Rogti, F.: Precieving of defect tolerance in perovskite absorber layer of efficient perovskite solar cell. Superlattices Microstruct. **129**, 240–246 (2019). https://doi.org/10.1109/ACCESS.2020.3000217

Hossain, M.I., Alharbi, F.H., Tabet, N.: Copper oxide as inorganic hole transport material for lead halide perovskite based solar cells. Sol. Energy **120**, 370–380 (2015a). https://doi.org/10.1016/j.solener.2015.07.040

Hossain, M.I., Fahhad, H., Alharbi, N.T.: Copper oxide as inorganic hole transport material for lead halide perovskite based solar cells. Sol. Energy **120**, 370–380 (2015). https://doi.org/10.1016/j.solener.2015.07.040

Huang, L., Sun, X., Li, C., Xu, R., Xu, J., Du, Y., Wu, Y., Ni, J., Cai, H., Li, J., Hu, Z., Zhang, J.: Solar Energy Mater. Solar Cells **157**, 1038–1047 (2016). https://doi.org/10.1016/j.solmat.2016.08.025

Hui-Jing, D., Wang, W.-C., Zhu, J.-Z.: Device simulation of lead free $Ch_3NH_3SnI_3$ perovskite solar cell with high efficiency. Chin Phys B **25**(10), 108808 (2016). https://doi.org/10.1088/1674-1056/25/10/108802

Hui-Jing, Du., Wang, W.-C., Zhu, J.-Z.: Device simulation of lead-free $CH_3NH_3SnI_3$ perovskite solar cells with high efficiency. Chin. Phys. B **25**(10), 25 (2016). https://doi.org/10.1088/1674-1056/25/10/108802

Kang, A.K., Zandi, M.H., Gorji, N.E.: Simulation analysis of graphene contacted perovskite solar cells using SCAPS-1D. Opt. Quant. Electron **51**(4), 91 (2019). https://doi.org/10.1007/s11082-019-1802-3

Karimi, E., Ghorashi, Bagher, M.: Simulation of perovskite solar cell with P_3HT as hole transport layer. J Nanophotonics **11**, 032514 (2017). https://doi.org/10.1117/1.JNP.11.032510

Ke, W., Kanatzidis, G.M.: Prospects for low-toxicity lead-free perovskite solar cells. Nat. Comm. **10**, 1–4 (2019). https://doi.org/10.1038/s41467-019-08918-3

Krishnamurthi, V., Khan, H., Ahmed, T., Zavabeti, A., Tawfik, S.A., Jain, S.K., Spencer, M.J.S., Walia, S.: Liquid-metal synthesized ultrathin sns layers for high-performance broadband photodetectors. Adv. Mater. **32**(45), 2004247 (2020a). https://doi.org/10.1002/adma.202004247

Krishnamurthi, V., Khan, H., Ahmed, T., Zavabeti, A., Tawfik, S.A., Mahmood, N., Walia, S.: Broadband photodetectors: liquid-metal synthesized ultrathin SnS layers for high-performance broadband photodetectors. Adv. Mater. **32**(45), 2070338 (2020b). https://doi.org/10.1002/adma.202070338

Lakhdar, N., Hima, A.: Electron transport material effect on performance of perovskite solar cells based on $CH_3NH_3GeI_3$. Opt. Mater. **99**, 109517–109521 (2019). https://doi.org/10.1016/j.optmat.2019.109517

Li, J., Shabbir, B., Wang, C., Wan, T., Ou, Q.G., Yu, P., Tadich, A., Jiao, X., Chu, D., Qi, D., Li, D., Kan, R., Huang, Y., Dong, Y., Jasieniak, J., Zhang, Y., Bao, Q.: Perovskite x-ray detectors: flexible, printable soft-x-ray detectors based on all-inorganic perovskite quantum dots. Adv. Mater. **31**, 1979214 (2019). https://doi.org/10.1002/adma.201970214

Liu, M., Johnston, M.B., Snaith, H.J.: Efficient planar heterojunction perovskite solar cells by vapor deposition. Nature **501**(7467), 395–403 (2013). https://doi.org/10.1117/1.JPE.9.021001

Liu, F., Zhu, J., Wei, J., Li, Y., Lv, M., Yang, S., Zhang, B., Yao, J., Dai, S.: Numerical simulation: toward the high efficiency planer perovskite solar cells. Appl. Phys. Lett. **104**, 253508–253508 (2014). https://doi.org/10.1063/1.4885367

Liu, J., Shabbir, B., Wang, C., Wan, T., Bao, Q.: Flexible, printable soft-x-ray detectors based on all-inorganic perovskite quantum dots. Adv. Mater. **31**(30), 1901644 (2019). https://doi.org/10.1002/adma.201901644

Liu, J., Chen, K., Khan, S.A., Shabbir, B., Zhang, Y., Khan, Q., Bao, Q.: Synthesis and optical applications of low dimensional metal-halide perovskites. Nanotechnology **31**, 152002 (2020). https://doi.org/10.1088/1361-6528/ab5a19

Minemoto, T., Murata, M.: Device modeling of perovskite solar cells based on structural similarity with thin film inorganic semiconductor solar cells. J. Appl. Phys. **116**, 054505–054505 (2014). https://doi.org/10.1063/1.4891982

Nayak, P.K., Mahesh, S., Snaith, H.J., Cahen, D.: Photovoltaic solar cell technologies analyzing the state of the art. Nat. Rev Mater. **4**, 269–285 (2019). https://doi.org/10.1021/acs.jpca.0c02912

Rai, S., Pandey, B.K., Dwivedi, D.K.: Modeling of highly efficient and low cost CH3NH3Pb(I1-xClx)3 based perovskite solar cell by numerical simulation. Opt. Mater. **100**, 109631–109639 (2020). https://doi.org/10.1016/j.optmat.2019

Ye, T., Fu, W., Wu, J., Yu, Z., Jin, X., Chen, H., Li, H.: J. Mater. Chem. A, **4**, 1214–1217 (2016). https://doi.org/10.1039/C5TA10155G

Younis, A., Hu, L., Sharma, P., Lin, C., Mi, Y., Guan, X., Zhang, D., Wang, Y., He, T., Liu, X., Shabbir, B., Huang, S., Seidel, J., Wu, T.: Enhancing resistive switching performance and ambient stability of hybrid perovskite single crystals via embedding colloidal quantum dots. Adv. Func. Mater. **30**(31), 2002948 (2020). https://doi.org/10.1002/adfm.202002948

Zekry, A., Shaker, A., Salem, M.: Solar cells and arrays: principles, analysis, and design. Adv. Renew. Energies Power Technol **1**, 562018 (2018). https://doi.org/10.1016/B978-0-12-812959-3.00001-0

Zou, H., Guo, D., He, B.: Enhanced photocurrent density of HTM-free perovskite solar cells by carbon quantum dots. Appl. Surf. Sci. **430**, 625–631 (2018). https://doi.org/10.1016/j.apsusc.2017.05.122